

Comparing thermal stimulation techniques in infrared thermographic inspection of corrosion in steel

A O Chulkov, V P Vavilov

National Research Tomsk Polytechnic University, Russia 634050, Tomsk, Lenin Av.,
30
chulkovao@tpu.ru

Abstract

Remote detection of corrosion in metals is a developing application area of active thermal nondestructive testing. In this study, emphasis is made on the optimization of heating techniques that is of a major interest in practical surveys. Some popular data processing techniques, such as Fourier transform, correlation and principal component analysis, are also quantitatively compared in application to corrosion detection in 1-2 mm thick steel by applying a criterion of signal-to-noise ratio. The best inspection results have been obtained by using powerful halogen lamps and air blowers. Material loss of about 25 % with lateral dimensions greater than 10×10 mm can be reliably identified in practical tests. The use of Xenon flash tubes is inefficient because of significant steel thickness. LED panels have not provided expected results due to low absorption of LED quasi-monochromatic radiation.

Keywords: active thermal nondestructive testing, corrosion detection, thermal stimulation, signal-to-noise ratio, image processing

1. Introduction

Remote detection of corrosion in metals is one of quickly developing application areas of active thermal nondestructive testing (TNDT). The results of earlier publications can be reduced to the following statements [1–14]: 1) the most successful applications are related to thin (1-2 mm) aluminum panels used in aviation and thicker (1-6 mm) steel components used in power production and petrochemical industry (in some cases, material loss can be detected in 10-15 mm-thick steel), 2) aluminum specimens are to be “black-painted” to enhance optical absorptivity/emissivity, even if the coating may be not really black in the visual wavelength band, 3) in most cases, optical thermal stimulation, in particular, by applying powerful Xenon tubes and halogen lamps, is considered as most appropriate, 4) acquisition frequency should be quite high in the case of aluminum (30–200 Hz) and “medium” if one deals with steel (10-30 Hz), 5) the theory of TNDT is well-developed to reveal basic relationships between surface temperature and defect parameters [6, 7, 10–12]; if defect lateral size is 6-10 times greater than specimen thickness (1D defects), a rather simple inversion formula allows fairly accurate estimation of material loss: $\Delta L/L = 1 - T_{nd}/T_d$, where T_{nd}, T_d are the specimen excess temperatures in defect and non-defect areas respectively; 3D defects can be identified by introducing some correction coefficients [1] or general inversion formulas [12], 6) the detection limit



of few percent of material loss has been reported in the inspection of aluminum [2–5], while, in the case of thick steel, the corresponding estimate is about 20 % [1, 8–11].

In this study, emphasis is made on the optimization of heating techniques that is of a major interest in practical surveys. Some popular data processing techniques are quantitatively compared in application to corrosion detection by using a criterion of signal-to-noise ratio (following the inspection philosophy described in [15, 16]).

2. TNDT of corrosion: recall to the basics

A ‘classical’ scheme of active one-sided TNDT is reminded in Figure 1. A sample with hidden corrosion is heated on the front surface (Figure 1a). Typically, a powerful pulse of optical radiation should be applied to quickly enhance surface temperature in non-defect and defect areas and then monitor these temperatures thermographically at the cooling stage; note that excess temperatures T_{nd} and T_d are counted from the initial temperature T_m that is typically the ambient temperature. Both defect detection and characterization are related to the analysis of differential temperature signals $\Delta T(\tau) = T_d(\tau) - T_{nd}(\tau)$ which evolve in time τ (Figure 1b). A maximum signal ΔT_m occurs at a particular time τ_m with both latter values being dependent on metal conductivity, material loss $\Delta L/L$, defect size and intensity of heat exchange with the ambient.

Three graphs in Figure 1b were calculated for the 1D material loss of 1 mm in a 5 mm-thick AISI 1010 steel by using Layer-3 Analytic software from Innovation, Ltd., Russia. In all cases, the injected energy was the same (10^4 J/m^2) but the heat pulse duration was 0.1, 1 and 10 s. In the first 2 cases, $\Delta T_m = 0.30 \text{ }^\circ\text{C}$, and only for the long (10 s) pulse the signal slightly decayed up to $0.28 \text{ }^\circ\text{C}$.

If heating time τ_h is relatively long, the time instant τ_m may occur within the heat pulse, i.e. $\tau_m < \tau_h$, or immediately after heating stopped as shown in the middle and bottom graphs of Figure 1b. This is an undesirable situation because temperature signals are often corrupted by strong reflection noise. Therefore, either a heat pulse should be short enough or stimulating energy should be out of the spectral range of a used infrared (IR) imager.

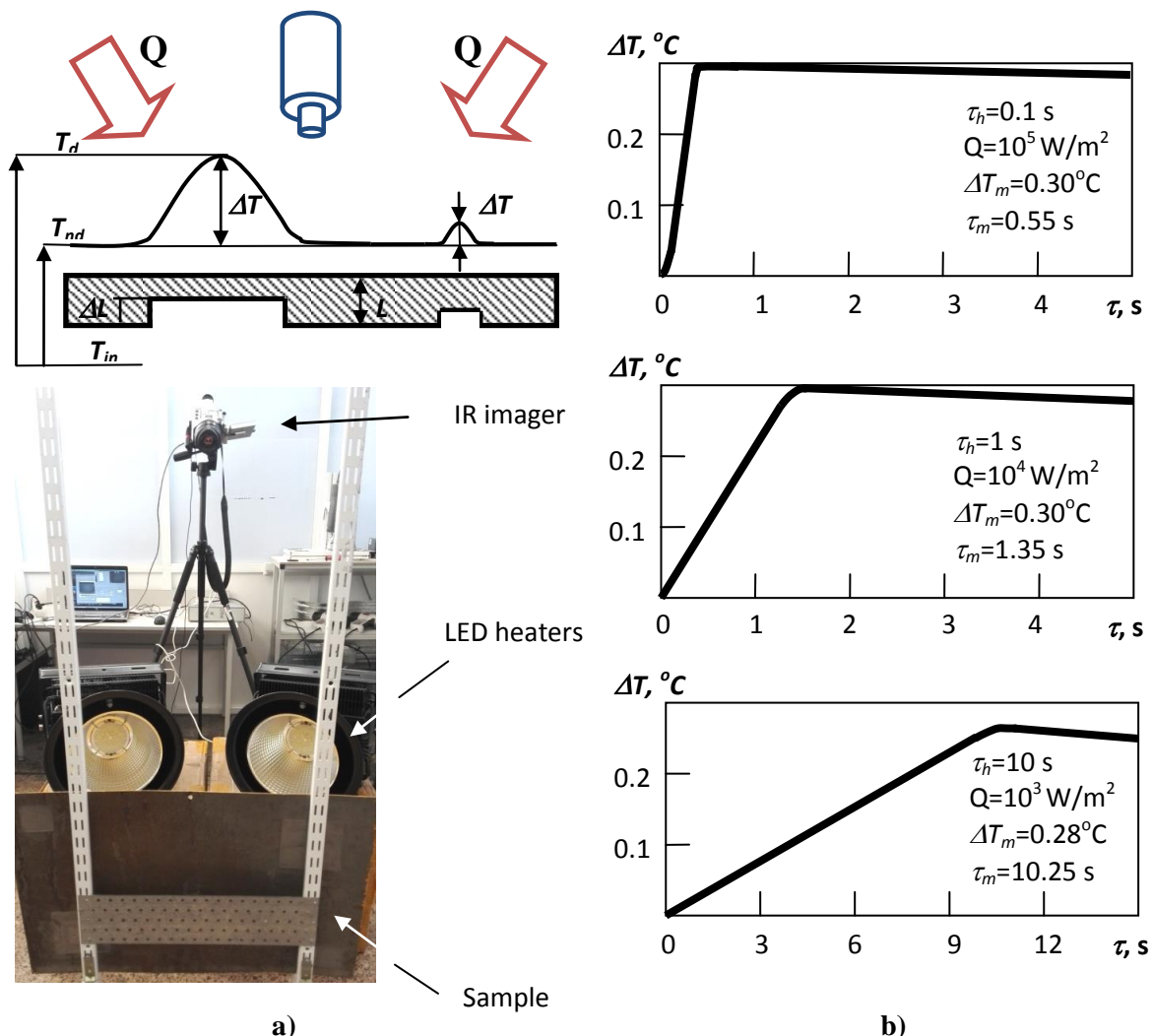


Figure 1. TNDT of hidden corrosion:
a – test scheme and experimental set-up,
b – evolution of temperature signals
(AISI 1010 steel, $L = 5$ mm, $\Delta L/L = 20$ %)

3. Experimental setup and test samples

The photo of the experimental set-up used in corrosion detection is shown in Figure 1a. A test sample with rear-surface corrosion has been thermally stimulated on the front surface with its dynamic temperature distribution being recorded with a TH-9100 IR imager from NEC Avio (image format 320×240, temperature resolution up to 30 mK, maximum acquisition frequency 60 Hz). Thermal stimulation sources have been the following: 1) two Xenon flash tubes with the total energy of 3.2 kJ delivered for 5 ms, 2) two halogen lamp sources with the total power of 2 and 30 kW, 3) two LED panels with the total power of 1 kW, 4) two air blowers with the total power of 4 kW.

Two 1 and 2 mm-thick reference samples made of AISI 1010 steel have been used to evaluate efficiency of corrosion detection by applying the above-mentioned heat sources. Some square-shaped bottom “holes” were manufactured to simulate corrosion areas of varying size and material loss (Figure 2a). Both samples were painted with a yellow acrylic dye to simulate containers used in nuclear engineering for keeping radioactive wastes (perspective application area for active IR thermography).

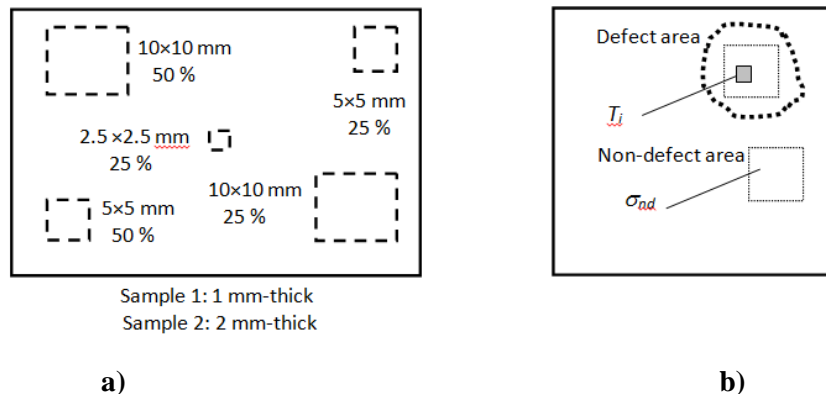


Figure 2. Reference sample scheme (a) and signal-to-noise concept (b).

4. Results and discussion

In TNDT, optimization of means of thermal stimulation is typically done on reference samples by using the signal-to-noise ratio criterion; also, mass/size parameters may be involved in consideration. Some other factors can be also taken into account, such as safety requirements; for instance, heaters with open filament may be not allowed for use close to petrochemical tanks.

Signal-to-noise ratio S is a convenient optimization parameter to compare inspection procedures and processing algorithms. When calculating S , one must choose both defect and non-defect areas thus making S as quantitative but subjective parameter (Figure 2b). The simplest formula for S is:

$$S = (\bar{T}_d - \bar{T}_{nd}) / \sigma_{nd}, \quad (1)$$

where \bar{T}_d , \bar{T}_{nd} are the mean temperatures, and σ_{nd} is the standard deviation of temperature in a non-defect area. The disadvantage of Eq. (1) is that, in some special cases, separate sections of defect areas can provide signals both higher and lower than the background thus decreasing their 'arithmetic' contribution to S . A more correct expression would be as follows:

$$S = \left[\sqrt{\sum_{i=1}^M (T_i - \bar{T}_{nd})^2 / M} \right] / \sigma_{nd}, \quad (2)$$

where T_i is the temperature (or any derivative signal) in the i -th pixel of a defect area, and M is the number of pixels in a chosen defect area.

Experimental results are illustrated with images in Figure 3. When applying flash heating, the acquisition frequency was 60 Hz (300 images in a sequence), in all other cases – 10 Hz (150 images in a sequence). All sequences have been processed by using the algorithms which are common in TNDT, namely: Fourier transform in time (pulse phase thermography), singular value decomposition (principle component analysis - PCA) and temporal correlation. To calculate S values, the corresponding square-shaped areas of interest were chosen on IR thermograms as shown in Figure 3.

The left column of images in Figure 3 is related to Sample 1 and the right one – to Sample 2. We remind that both sample contained the areas of simulated corrosion with the same material loss, so the only difference between results was in sample thickness. Visual perception of data in Figure 3 allows the following conclusions: 1) in accordance with the TNDT theory, the corrosion areas look warmer than the non-defective ones in raw images, while the processed images are characterized by 'defective' signals both higher and lower than the background, 2) all image processing techniques are based on the analysis of temperature evolution in time and lead to considerable reduction of uneven heating phenomena, 3) the visually best results appear when stimulating samples with the 30 kW halogen lamps and the 4 kW air blowers (in the latter case, absorptivity/emissivity phenomena are less

significant in comparison to optical heating), 4) independently on sample thickness, material loss of 25 % with lateral dimensions greater than 10×10 mm can be reliably identified; smaller size defects can be also seen but probability of correct detection may be low.

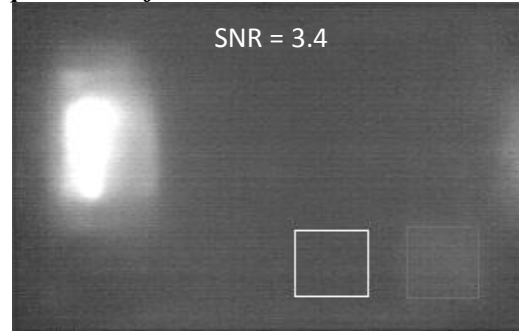
Sample 1 (1 mm-thick)

Sample 2 (2 mm-thick)

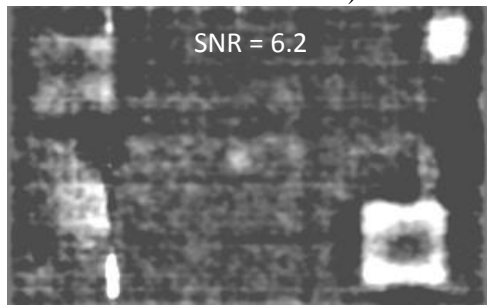
Heating with 2 halogen lamps 2×1 kW for 10 s



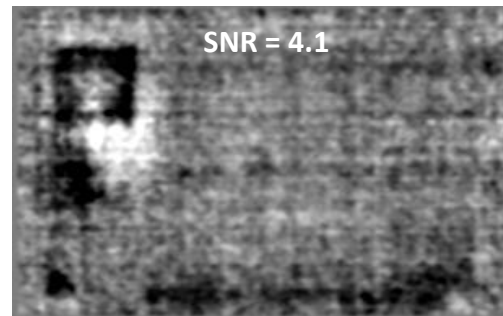
Raw image (sample deformation is seen on the left)



Raw image



PCA image

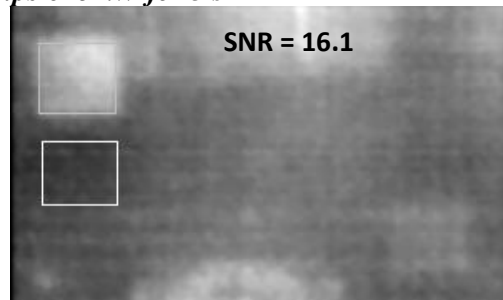


PCA image

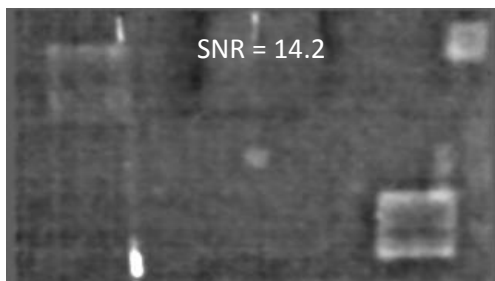
Heating with 6 halogen lamps 6×5 kW for 3 s



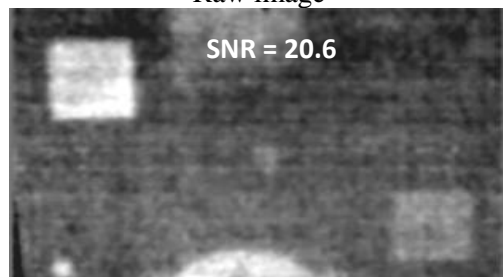
Raw image



Raw image



PCA image



PCA image

Figure 3. Image processing in the inspection of steel reference samples (to continue)

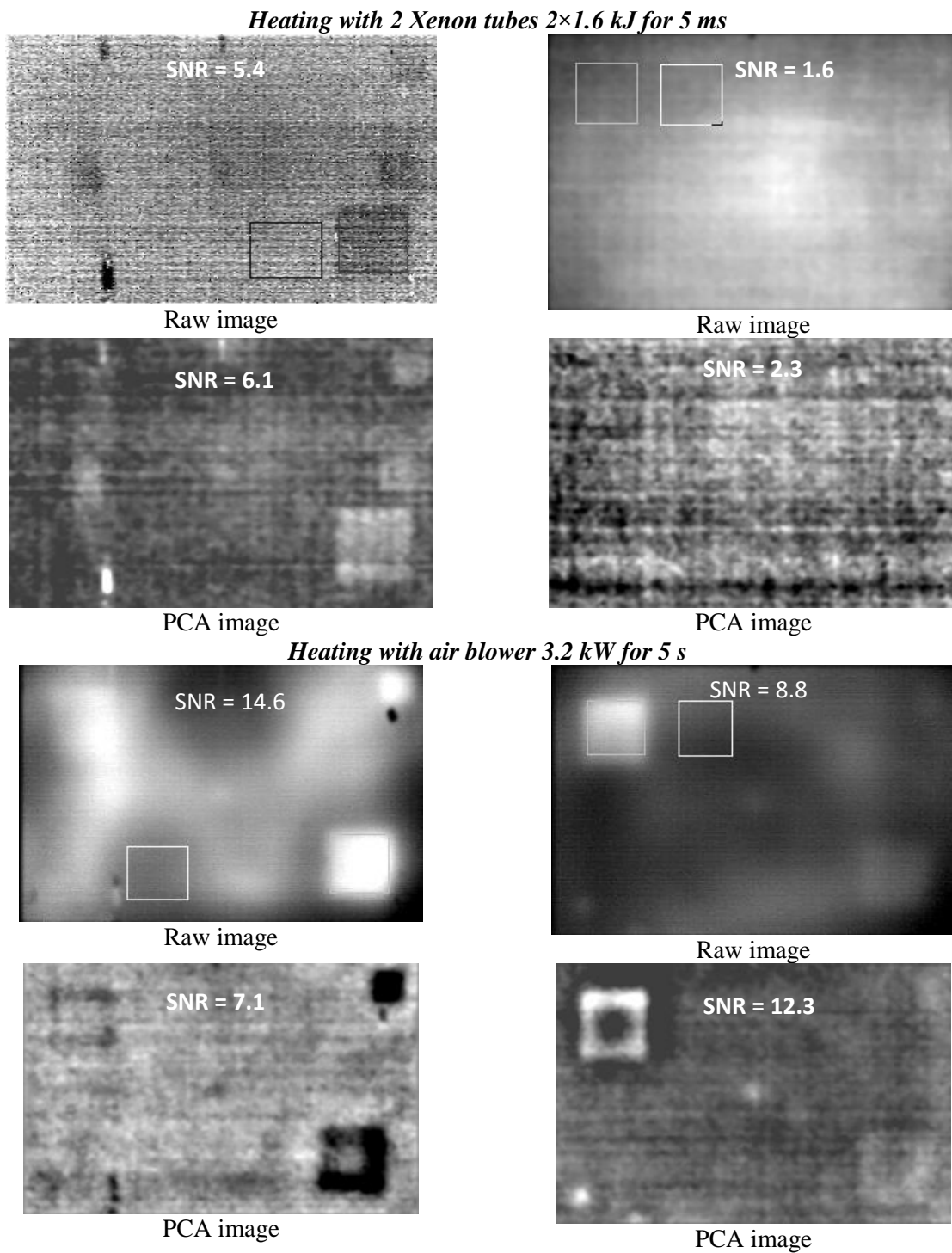


Figure 3. Image processing in the inspection of steel reference samples (to continue)

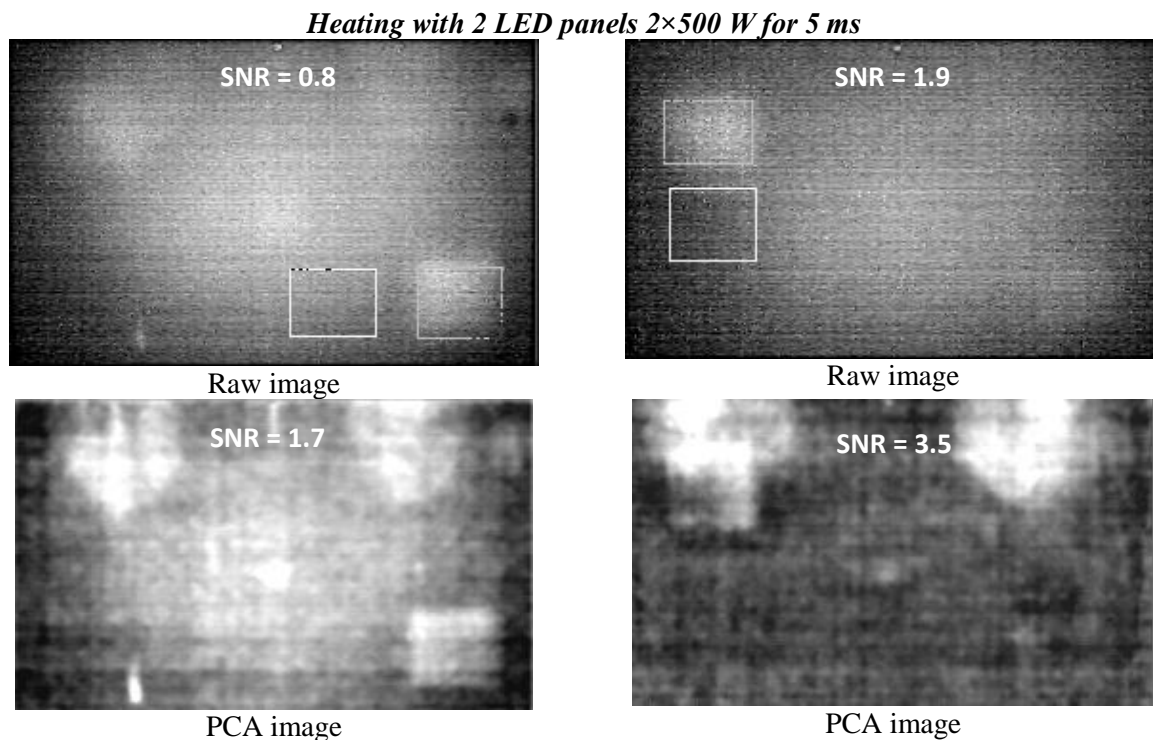


Figure 3. Image processing in the inspection of steel reference samples (continued)

The evaluation of experimental results by signal-to-noise ratio that is presented in Figure 4 leads to the same conclusions. The highest S values have been from 11 to 20,6 thus ensuring reliable detection of the corresponding defects. It is interesting that in some cases S values are higher in raw images than after processing but the visual perception of images is always in favor of image processing. This can be explained by a relatively small size of chosen defect and non-defect areas, while advantages of image processing appear in the processing of large format images. Besides, S values involve single pixel amplitudes without taking into account image texture heuristically evaluated by an operator.

The low efficiency of Xenon tubes can be explained by the significant thickness of the steel samples; this stimulation technique seems to be fairly good in the inspection of thin aluminum sheets. It is important noting the unsatisfactory results obtained with LED panels. This finding does not support the hopes of improving test results by using quasi-monochromatic LED radiation of which spectrum (about 0.7 μm) is far away from the spectral range of typical IR imagers (2–5 and 7–13 μm) thus producing no reflection noise. However, in our case, the absorption of the LED radiation by yellow-painted samples has been too low to build-up appropriate temperature signals.

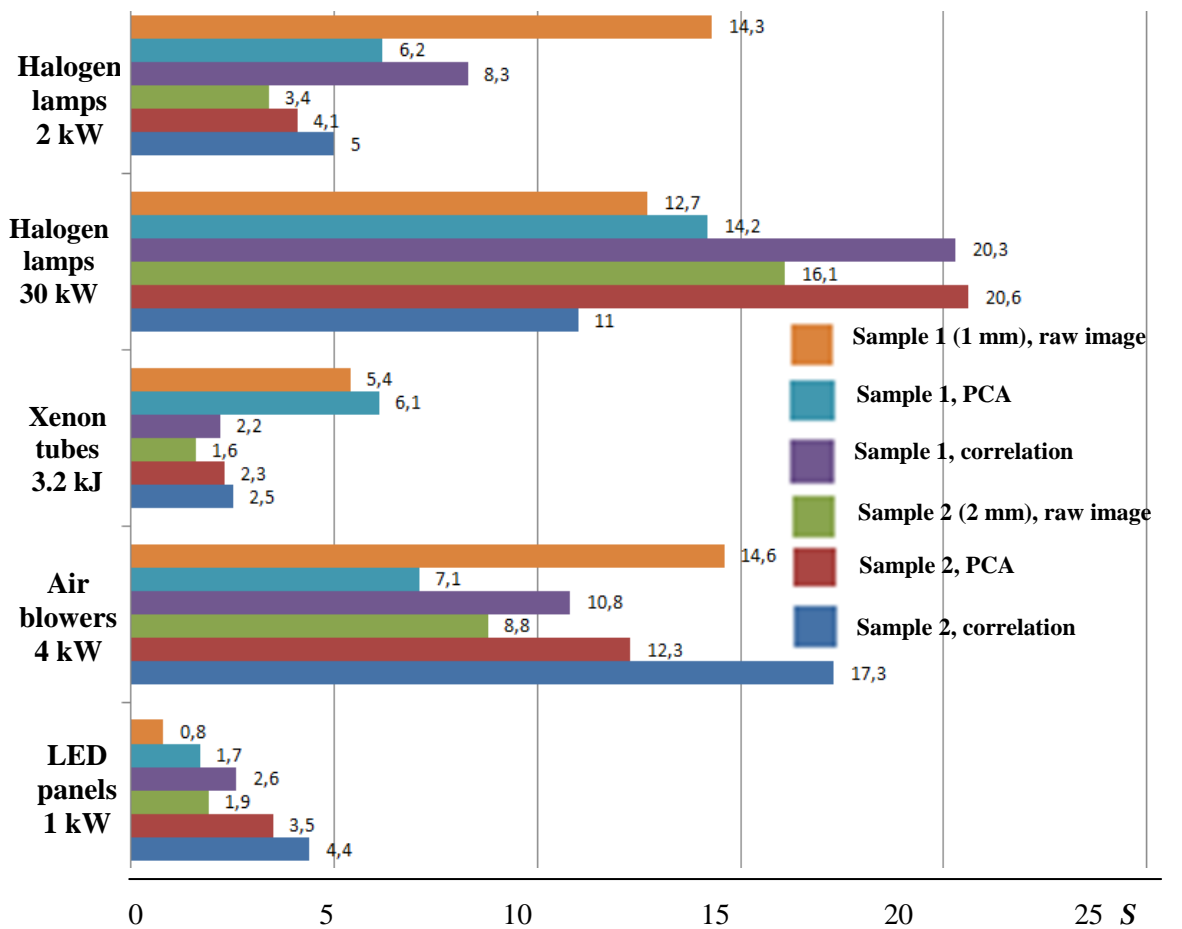


Figure 4. Evaluating thermal stimulation efficiency in corrosion detection.

5. Conclusion

The practical efficiency of several thermal stimulation techniques has been evaluated in the detection of hidden corrosion in 1–2 mm thick steel samples. Signal-to-noise ratio has been chosen as a comparison criterion to show that the best results are ensured when using powerful halogen lamps and air blowers (a required stimulation power is of some kW). Material loss of about 25 % with lateral dimensions greater than 10×10 mm can be reliably identified in practical surveys. The use of Xenon flash tubes with energy of few kJ is inefficient because of significant steel thickness. LED panels have not provided expected results due to low absorption of quasi-monochromatic LED radiation.

This research was supported by the NIR # 445 (ONG), State order of the Russian Ministry of Higher Education for 2014-2016.

References

- [1] Vavilov V P, Chulkov A O, Burleigh D. 2012 *Proc. SPIE Thermosense-XXXIV* vol. 8354 pp 835401–835409
- [2] Prabhu D R, Winfree W P 1993 *Rev. Progress in Quant. NDE* vol. 12 pp 1260–1265
- [3] Syed HI, Winfree W P, Cramer K E, Howell P A 1993 *Rev. of Progress in Quant. NDE* vol.12 pp 724–729
- [4] Alcott J 1994 *Mater. Evaluation* **5** pp 64–73
- [5] Prati J 2000 *Proc. SPIE* vol. 4020 pp 200–209

- [6] Vavilov V, Grinzato E, Bison P G, Marinetti S and Bales M 1996 *Intern. J. Heat & Mass Transfer* vol. 39 pp 355–371
- [7] Grinzato E and Vavilov V 1998 *Rev. Generale Termique* vol. 37 **8** pp 669–679
- [8] Vavilov V, Shiryaev V and Grinzato E 1998 *Insight* vol. 40 **6** pp 408–410
- [9] Vavilov V P, Nesteruk D A, Chulkov A O, Shiryaev V V 2013 *Rus. J. NDT* vol. 49 **11** pp 619–624
- [10] Grinzato E, Bison P, Marinetti S and Vavilov V 2006 *Proc. SPIE* **6205** 620517
- [11] Grinzato E, Vavilov V, Bison P G and Marinetti S 2007 *Infrared Physics & Technology* 49 pp 234–238
- [12] Marinetti S and Vavilov V 2010 *Corrosion science* vol. 52 **3** pp 865–872
- [13] Lugin S and Netzelmann U 2007 *NDT & E Intern* vol. 40 pp 220–228
- [14] Woolard D F and Cramer K E 2004 *Proc. SPIE Thermosense-XXVI* vol. 5405 pp 366–373
- [15] Vavilov V P 2011 *Proc. of the Fall 2011 ASNT Conf.* 8 p.
- [16] Albendea P, Madruga F J, Cobo A, López-Higuera J M 2010 *Proc. 10th Intern. Conf. on Quant. Infr. Therm.* 8 p